

Bipartite Discrete Time Crystals on Decorated Lattices

Lennart Fernandes,^{1,*} Joseph Tindall,² and Dries Sels^{1,2}

¹*Center for Quantum Phenomena, Department of Physics,
New York University, New York, NY 10003, USA*

²*Center for Computational Quantum Physics, Flatiron Institute, New York, NY 10010, USA*

We study time-crystalline order in periodically driven quantum Ising models on disorder-free decorated lattices. Using a tensor network ansatz for the state which reflects the geometry of a unit cell of the lattice, we show through finite entanglement scaling that the system has an exponentially long-lived subharmonic response in the thermodynamic limit. The resulting discrete time crystal is not only stable to imperfections in the transverse field, but also exhibits a bipartite rigidity to generic perturbations in the longitudinal field. We call this state a bipartite discrete time crystal and reveal a rich prethermal phase diagram, including multiple regions of bipartite time-crystalline order, uniform time-crystalline order and thermalization, with boundaries depending delicately on the topology of the decorated lattice. Our results thus uncover a variety of time crystals which may be realized on current digital quantum processors and analog quantum simulators.

Introduction. — The stable crystalline structure of solid materials is a striking example of spontaneous symmetry breaking, as the ground state violates spatial translational invariance in the formation of a periodic lattice. The temporal counterpart of this phenomenon, a state which evolves periodically in time, constitutes a breaking of time translational invariance which has been coined a *time crystal* [1]. While the spontaneous breaking of a continuous time symmetry by an isolated quantum system in equilibrium was proven to be impossible [2–4], out-of-equilibrium states which break a discrete time translational invariance can be realized in Floquet systems, where an external drive modulates the governing Hamiltonian over a period τ , $\mathcal{H}(t) = \mathcal{H}(t + \tau)$ [5–7]. In this case, the discrete time symmetry imposed by the periodic drive is broken when observables do not reach a steady state at stroboscopic times $t = n\tau$, but instead exhibit long-lived periodicity at a lower frequency,

$$|\psi(t)\rangle = |\psi(t + \tilde{n}\tau)\rangle, \quad (\tilde{n} > 1). \quad (1)$$

When stable to generic local perturbations, such symmetry-broken states are called *discrete time crystals* (DTC) [8, 9] due to the spontaneous emergence of subharmonic order. The primary obstacle for constructing long-lived DTCs is the absorption of energy injected by the Floquet drive, which causes the system to relax to an infinite temperature equilibrium state. With the exception of many-body localized systems [10–16] and systems prepared in quantum-scarred eigenstates [17–20], discrete time crystals in clean, non-integrable systems are therefore a transient phenomenon. Nevertheless, the inverse exponential scaling of the absorption rate with the driving frequency [21, 22] allows for long-lived *prethermal* DTCs [23, 24], and several mechanisms have been proposed to extend the lifetime of time-crystalline

order beyond the limiting case of a high driving frequency [9, 25]. Among them is the presence of a confining potential, which, in analogy to the confinement of quarks in QCD [26, 27], causes magnetic domain walls to form bound states as a result of the energy cost associated with the growth of the domain [28–30]. The consequently inhibited spread of correlations was found in a variety of systems to delay the onset of thermalization [31–33], and shown to allow for long-lived time-crystalline order in the case of confinement by an external field in a one-dimensional Ising chain [34]. Since symmetry-broken states of ferromagnetic models in higher dimensions generically exhibit confinement due to the growth of a domain wall with the size of the domain itself [33, 35], disorder-free DTCs have been predicted to occur in the two-dimensional square Ising model [36], and were recently observed on a digital quantum processor with a decorated hexagonal geometry [37]. In the latter system, both Floquet dynamics and non-thermal dynamics caused by confinement of excitations have been accurately reproduced through tensor network state (TNS) simulations employing belief propagation [33, 38].

We build upon these successes to study the emergence, stability and lifetime of time-crystalline order in the Floquet Ising model on generic decorated lattice structures. By employing a tensor network reflecting the unit cell of an infinite realization of the lattice, optimized with belief propagation, we are able to directly access the thermodynamic limit. Supported by state vector simulations on finite graphs, this will lead us to introduce *bipartite* discrete time crystals and construct a prethermal phase diagram hosting several DTC regimes determined by the lattice topology.

Model and approach. — We consider the Ising model in the presence of both transverse and longitudinal magnetic fields, described by the Hamiltonian

$$\mathcal{H} = h_x \sum_j X_j + h_z \sum_j Z_j - J \sum_{\langle jk \rangle} Z_j Z_k, \quad (2)$$

* lf2680@nyu.edu

where X and Z are the spin-1/2 Pauli operators. Both the interaction strength J and the fields h_x and h_z are taken to be uniform, while the summations j and $\langle jk \rangle$ run over all sites and nearest-neighbor links of the underlying decorated lattice. We define a decorated lattice as one in which each of the edges of a lattice with vertices of uniform coordination number z is decorated with an additional vertex, with the example of the decorated hexagonal lattice shown in Fig. 1(a). A distinguishing feature of this geometry is its bipartite structure, comprising two distinct sublattices of vertices with degree 2 and $z > 2$. We will refer to these sublattices as the A - and B -lattices, respectively. A discrete time symmetry is introduced by the periodically driven dynamics illustrated in Fig. 1(b), in which unitary time evolution over the period τ of a single Floquet cycle is generated by successive application of the three contributions to the Hamiltonian. Setting $\hbar = 1$ and defining the rotation operator of an operator O as $R_O(\theta) = e^{-i\theta O/2}$, we can write this Floquet unitary as

$$U(\tau) = \left[\prod_j R_X^j(\theta_x) \right] \left[\prod_j R_Z^j(\theta_z) \right] \left[\prod_{\langle jk \rangle} R_{ZZ}^{jk}(\theta_J) \right], \quad (3)$$

where the finite rotation angles are related to the Hamiltonian and the Floquet period as $\theta_J = -2J\tau$, $\theta_x = 2h_x\tau$ and $\theta_z = 2h_z\tau$. To compute the dynamics induced by $U(\tau)$ on a given decorated lattice in the thermodynamic limit, we use the BP-iTNS ansatz. Specifically, we simulate the dynamics on the $K_{2,z}$ complete bipartite graph [39], using a tensor network state (TNS) whose structure matches that of the $K_{2,z}$ graph. The application of two-site gates and the measurement of expectation values is done via belief propagation (BP), which works by identifying vectorized message tensors as a rank-1 approximation for the environments in the tensor network [38, 40–43]. These BP-iTNS results are exactly equivalent [33, 38, 44] to those obtained by simulating the dynamics of the full decorated lattice in the thermodynamic limit with a TNS matching the infinite lattice and optimized with BP. The error made by the BP approximation decreases exponentially with the size of the smallest loop in the system, making it especially suitable for the considered geometries due to the fact the decorations double the smallest loop size in the original lattice. Within the limitations set by the bond dimension of the iTNS and the loop corrections neglected by the BP approximation, the BP-iTNS ansatz allows us to access the dynamics induced by $U(\tau)$ on any decorated lattice structure in the thermodynamic limit. We picture this ansatz for the decorated hexagonal ($z = 3$) and decorated square (Lieb) lattice ($z = 4$) in Fig. 1(c-d).

Time-crystalline order. — We consider the system initialized in the symmetry-broken product state $|\uparrow\rangle^{\otimes(z+2)}$ and subject to an effective confining potential through interactions taken to be maximally entangling

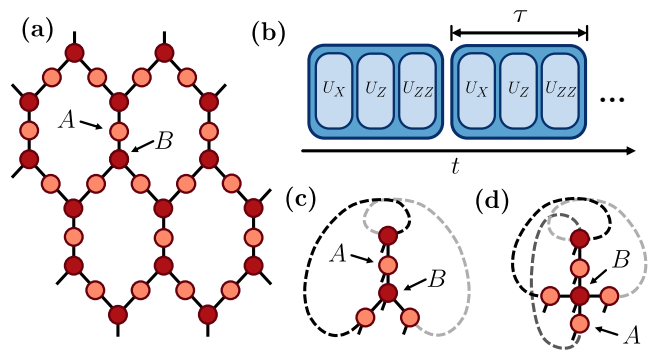


FIG. 1. **Geometry and dynamics.** (a) The two-dimensional decorated hexagon lattice consists of two sublattices of sites with two (A , light) and three (B , dark) nearest neighbors. (b) Unitary sequence of two Floquet cycles. (c) The complete bipartite graph $K_{2,3}$ as the BP-iTNS unit cell of a decorated hexagonal lattice, with periodic boundaries (dashed lines). (d) The $K_{2,4}$ unit cell of a Lieb lattice.

two-qubit rotations $\theta_J = -\pi/2$ at a vanishing longitudinal field $\theta_z = 0$. For a transverse field $\theta_x = \pi$, the dynamics consist of R_{ZZ} interactions alternating with a π -flip of all qubits around the X -axis, resulting in a perfect time-crystalline order of the magnetization with a subharmonic period 2τ ,

$$\langle \psi(n\tau) | Z | \psi(n\tau) \rangle = (-1)^n. \quad (4)$$

For any imperfect drive $\theta_x \neq \pi$, the system leaves the Z -polarized state and eventually thermalizes. However, as the stroboscopic dynamics in the limit $\theta_x \rightarrow \pi$ are governed to lowest order by a static Ising Hamiltonian, confinement dramatically slows down the absorption of energy and generation of entanglement [33], delaying thermalization during a prethermal time-crystalline stage.

Figure 2(a-c) shows the time evolution of the magnetization $\langle Z \rangle$ in the A -sublattice of a decorated hexagonal lattice subject to Floquet dynamics at three different transverse field drives $\theta_x/\pi = \{0.65, 0.75, 0.85\}$. For rotation angles deviating significantly from the perfect π -periodic drive as in Fig. 2(a), $\langle Z \rangle$ dephases rapidly as the system relaxes to an infinite temperature state. Conversely, Fig. 2(c) reveals a long-lived subharmonic response in the limit $\theta_x \rightarrow \pi$, signaling the emergence of a discrete time crystal. A crossover between these dynamical regimes of DTC order and thermalization was recently observed in error-mitigated quantum simulations on IBM's Heron architecture [37]. We develop a more exhaustive picture of this crossover directly in the thermodynamic limit by plotting in Fig. 2(d) the mean oscillation amplitude \bar{Z} averaged over 100 cycles of the Floquet unitary (3). In agreement with the dynamics illustrated in Fig. 2(a-c), the amplitude reaches zero as θ_x approaches $\pi/2$, and converges to unity in the limit $\theta_x \rightarrow \pi$. In the latter regime, the insensitivity of the finite magnetization to the bond dimension χ of the employed BP-

iTNS implies that entanglement growth is suppressed, consistent with the presence of an effective confining potential. For intermediary values of θ_x , a slow convergence with respect to χ indicates that the system becomes highly entangled as it crosses over into the thermalizing regime. The scaling of the entanglement entropy $S_E \propto \ln(\chi)$ allows us to estimate the magnetization at an unbounded S_E by extrapolating our results at finite χ to the limit $1/\ln(\chi) \rightarrow 0$. The linear scaling of the magnetization with this quantity is illustrated in the inset, and results in the full black lines in Fig. 2(a-d). The slope $\partial\bar{Z}/\partial[1/\ln(\chi)]$ of this finite entanglement scaling, plotted in Fig. 2(e), reaches a maximum which converges at late times to $\theta_x^*/\pi \approx 0.73$ (see Appendix A), providing an estimate of the crossover between DTC and thermalizing dynamics in agreement with the range $\theta_x^*/\pi \sim 0.7 - 0.8$ inferred from direct quantum simulation [37]. Moreover, this scaling analysis shows that the rate of entanglement production in the DTC regime decays exponentially with $1/|\theta_x - \pi|$. While the drift of the exponent γ over time indicates the eventual thermalization for any $\theta_x < \pi$, the inset of Fig. 2(e) shows that this occurs at most logarithmically in time, suggesting a prethermal DTC lifetime which grows exponentially in $1/|\theta_x - \pi|$.

Bipartite rigidity. — A comparable decay of the order parameter and $\theta_x^*/\pi \sim 0.6 - 0.8$ were previously inferred through matrix product state (MPS) simulations on finite square lattices [36], indicating that prethermal subharmonic oscillations are not specific to decorated lattice structures. However, true time-crystalline order requires, besides a robustness of the subharmonic response to an imperfect periodic drive, a self-stabilizing rigidity with respect to generic local perturbations [8]. We therefore extend the Floquet unitary (3) to include a finite longitudinal field $\theta_z > 0$. Where the interference of two driving fields will cause a generic system to exhibit a beating, a system in a stable time-crystalline phase retains its subharmonic response. Figure 3(a) shows the response of $\langle Z \rangle$ on both sublattices of a decorated hexagonal lattice to a transverse drive of $\theta_x = 0.85\pi$ within the time-crystalline regime, perturbed by a longitudinal field rotation $\theta_z = 0.4\pi$. This configuration was reported in Ref. [37] to cause a beating in the global magnetization, signalling the emergence of a discrete time quasi-crystal (DTQC) [45–47]. However, we find that the different connectivity of qubits in either sublattice results in qualitatively different behavior. Whereas qubits in the A -lattice exhibit a beating frequency manifesting as an envelope to the subharmonic response, a similar breaking of DTC order into quasi-crystalline dynamics is absent in the B -lattice, which is insensitive to longitudinal perturbations. This bipartite rigidity occurs for all values of $\theta_z \in [0, \pi]$, as illustrated by the power spectra in Figs. 3(b-d). While the peak of the subharmonic response at $\omega\tau = \pi$ remains unperturbed by the longitudinal field in the B -sublattice, the instability in the A -lattice causes a splitting into two

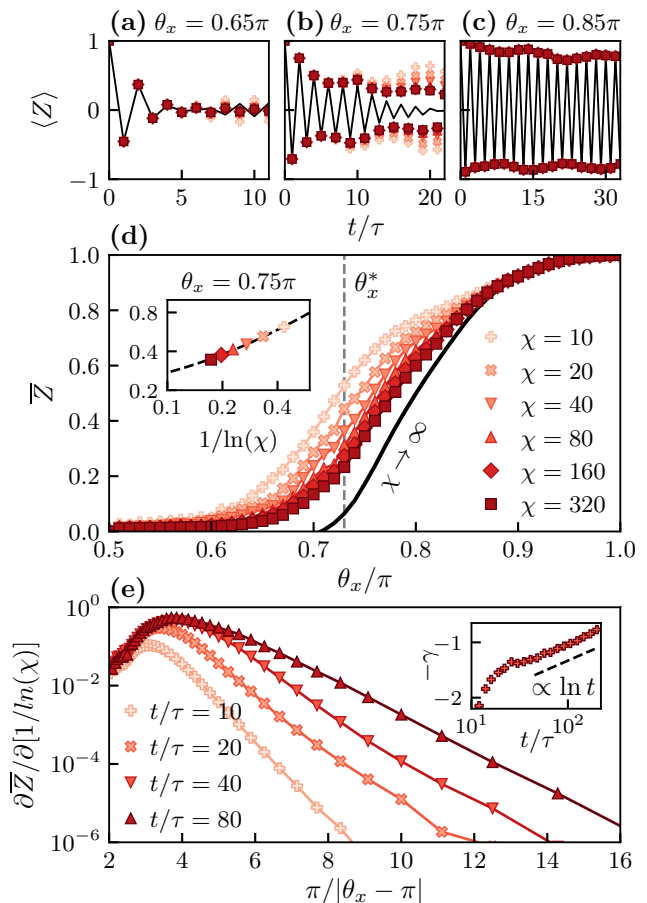


FIG. 2. **Time-crystalline order.** (a-c) Evolution of the magnetization on an infinite decorated hexagonal lattice for a periodic transverse field drive in the thermalizing (a), crossover (b) and DTC regime (c), evaluated at the bond dimensions shown in (d). (d) Mean magnetization in the thermodynamic limit as a function of θ_x , averaged over the first 100 cycles at different bond dimensions. The inset illustrates for $\theta_x = 0.75\pi$ the extrapolation $1/\ln(\chi) \rightarrow 0$, resulting in the full black line in panels (a-d). The crossover value θ_x^* inferred from a finite entanglement scaling is shown by the grey dashed line in (d). (e) Slope of the extrapolation for different number of Floquet cycles, decaying exponentially with $1/|\theta_x - \pi|$. The inset shows the evolution of the exponent.

peaks separated by $\delta\omega \propto \theta_z$. Since both sublattices exhibit reversible oscillatory dynamics, the entanglement entropy remains low. As shown by the crosses in Fig. 3(a) and dashed lines in Fig. 3(b-d), this property allows us to observe all qualitative features even from the evolution of a product state ($\chi = 1$), suggesting that the bipartite response is not caused by intricate many-body dynamics, but is instead a necessary feature of the decorated lattice topology. In Appendix B, we crosscheck the validity of our BP-iTNS method with exact state vector simulations of complete regular graphs with decorated edges, demonstrate the absence of rigidity in the corresponding undecorated lattices, and show that bipartite rigidity is

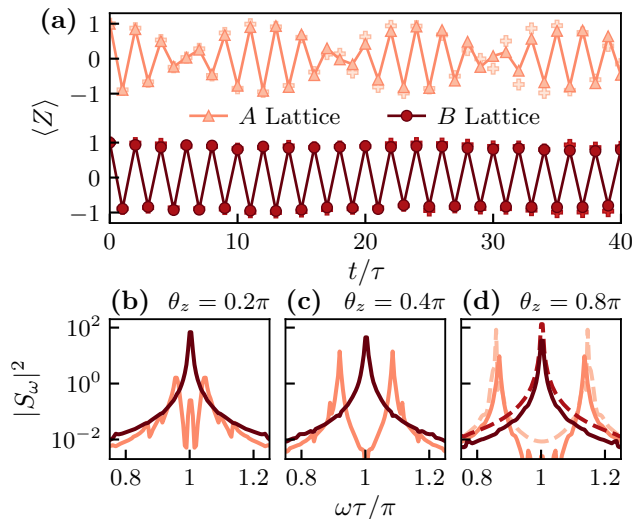


FIG. 3. **Bipartite rigidity.** (a) Time evolution of $\langle Z \rangle$ on the A- (top) and B-sublattice (bottom) of a decorated hexagonal lattice for $(\theta_J, \theta_x, \theta_z) = (-0.5\pi, 0.85\pi, 0.4\pi)$, calculated in the thermodynamic limit at $\chi = 160$. (b-d) Power spectra of the harmonic response for $\theta_x = 0.85\pi$ and $\theta_z/\pi = \{0.2, 0.4, 0.8\}$. The crosses in (a) and dashed lines in (d) indicate the corresponding result for $\chi = 1$.

not found in decorated square lattices ($z = 4$). Being a feature unique to systems with a bipartite topology, we thus define a *bipartite DTC* as a nonequilibrium state of matter in which the inhibition of entanglement growth results in a robust subharmonic response in an extensive part of, but not all of, the system.

Prethermal phase diagram. — The decorated lattice topology not only causes a bipartite rigidity to perturbations, but crucially determines the presence of time-crystalline order in the transverse field Ising model even at $\theta_z = 0$. To illustrate this, we extend the result of Fig. 2(d) to arbitrary interaction strengths θ_J and construct a prethermal phase diagram in the (θ_x, θ_J) parameter space. We distinguish a rigid subharmonic response from enveloped oscillations by defining the spectral power density $|S_\omega^{A/B}|^2$ at the subharmonic peak $\omega\tau = \pi$ as a prethermal DTC order parameter in either sublattice of the bipartite geometry. For a decorated hexagonal lattice, this gives rise to the diagrams shown in Fig. 4(a-b). In the weakly interacting limit $\theta_J \rightarrow 0$, the onset of interactions induces confinement which stabilizes subharmonic periodicity in the presence of increasingly perturbed π -flips, resulting in a sharp crossover to a state of time-crystalline order, which grows linearly with $|\theta_J|$ in both sublattices. The stabilizing effect of interactions stagnates around $\theta_J \approx -\pi/3$. Beyond this point, the range of perturbations $|\theta_x - \pi|$ to which the time crystal is robust shrinks until the eventual disappearance of DTC order in the node at $\theta_J = -2\pi/3$, followed by a revival at larger interaction strengths.

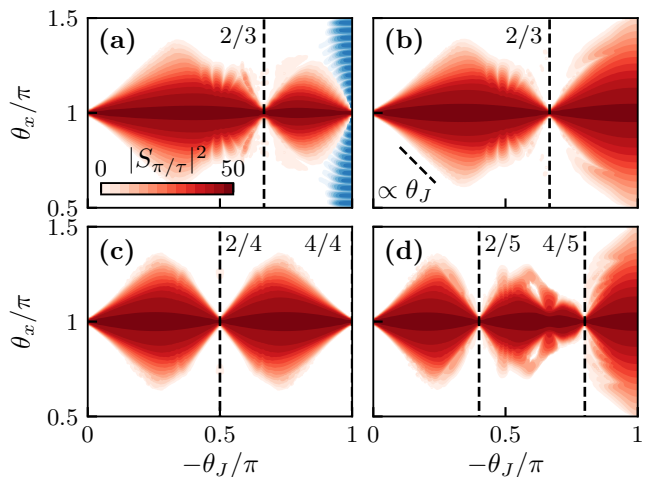


FIG. 4. **Prethermal phase diagrams.** (a-b) Spectral power density $|S_\omega|^2$ at the subharmonic peak $\omega\tau = \pi$ in the A- (a) and B-sublattice (b) of the Floquet Ising model ($\theta_z = 0$) in the decorated hexagonal lattice, evaluated over 50 Floquet cycles in the limit $\chi \rightarrow \infty$. Red regions indicate the presence of DTC order, while the blue region in (a) represents the spectral density of the largest non-subharmonic peak, indicating quasi-crystalline enveloped oscillations. (c-d) Subharmonic spectral power density $|S_{\pi/\tau}|^2$ in the B-sublattice of a Lieb lattice (c) and decorated 5-regular graph (d).

As seen from the spectral density $|S_{\pi/\tau}^B|^2$ of the subharmonic response in the thermodynamic limit of a Lieb lattice ($z = 4$) and decorated 5-regular graph ($z = 5$) shown in Fig. 4(c-d), the recurring appearance and disappearance of DTC order as a function of θ_J is a general feature of decorated lattice structures. In particular, nodes of vanishing DTC order occur at values $\theta_J = -2n\pi/z$, with $n \in \mathbb{N}$ and z the connectivity of the B-lattice. This is intuitively explained by the fact that the effective rotation experienced by a z -connected qubit in the B-lattice upon the application of z R_{ZZ} gates is then $2n\pi$, reintroducing the instability of a non-interacting model. By the same reasoning, the order parameter in the A-sublattice of any decorated lattice reaches a node at $\theta_J = -\pi$, as in Fig. 4(a). However, while nodes of the B-lattice occur also in the phase diagram of the A-lattice and thus destabilize DTC order in the entire system, the A-lattice node at $-\pi$ results in a regime of bipartite DTC order: qubits in the B-lattice [Fig. 4(b)] exhibit a robust subharmonic response in the limit $\theta_J \rightarrow -\pi$, whereas the A-lattice [Fig. 4(a)] acquires a quasi-crystalline beating similar to the dynamics in Fig. 3. This is shown by the blue-shaded amplitude of the largest non-subharmonic peak in the spectral density $|S_\omega^A|^2$ in Fig. 4(a). Finally, we note that bipartite DTCs do not appear in decorated square lattices with an even coordination number $z = 4$ in the B lattice. This follows from the above argument and is visible from the B-lattice order parameter in the Lieb lattice shown in Fig. 4(c), where the coincidence of

DTC nodes in both sublattices at $\theta_J = -\pi$ inhibits the revival of bipartite DTC order witnessed in decorated hexagonal and 5-regular graphs.

Conclusion and outlook. — Through tensor network simulations in the thermodynamic limit, we have studied discrete time crystals in periodically driven Ising models on decorated lattices. We have established that prethermal DTC order decays in a non-perturbative fashion from small deviations from the ideal π -periodic drive, and have found that the sensitivity to a longitudinal field, observed on a finite decorated hexagonal lattice in Ref. [37], manifests itself in only one of the two sublattices comprising a generic decorated graph structure. The latter observation implies the existence of a state of bipartite time-crystalline order, in which an extensive part of a bipartite system resisting thermalization displays subharmonic dynamics robust to generic local perturbations. Finally, we have constructed a prethermal DTC phase diagram for the specific cases of a decorated hexagonal lattice, Lieb lattice and decorated 5-regular lattice, uncovering a decay and resurrection of (bipartite) DTC order at interaction strengths determined by the topology of the graph.

The bipartite discrete time crystals we have introduced bear a resemblance to the notion of boundary time crystals (BTC) [48–50] and topological Floquet phases of edge states [51]. In contrast to these phenomena, bipartite DTCs as introduced in this work are distinguished by their extensive scaling with system size. As such, we anticipate experimental realizations of this phenomenon not only on current digital quantum processors [51–56], but also on atomic systems with tunable lattice structures [57–59] and condensed matter platforms with non-trivial topologies, such as spin impurities in diamond [47, 60]. Finally, additional research is required to explore whether the phenomenology presented here can be extended to the breaking of a continuous time symmetry in driven-dissipative systems [61–64] with a bipartite geometry.

Acknowledgements. — We thank Flaviano Morone, Michiel Wouters, Kilian Seibold and Berislav Buča for insightful discussions. L.F. was supported by a Philips postdoctoral fellowship of the Belgian American Educational Foundation. J.T. and D.S. are grateful for ongoing support through the Flatiron Institute, a division of the Simons Foundation. D.S. and L.F. are partially supported by AFOSR (Award no. FA9550-21-1-0236) and NSF (Award no. OAC2118310). The code used to produce the numerical results in this paper was written using the `ITensorNetworks.jl` package [65], a general purpose and publicly available Julia [66] package for manipulating tensor network states of arbitrary geometry. It is built on top of `ITensors.jl` [67], which provides the basic tensor operations. This work was supported in part through the NYU IT High Performance Computing resources, services, and staff expertise.

-
- [1] F. Wilczek, *Phys. Rev. Lett.* **109**, 160401 (2012).
 - [2] P. Bruno, *Phys. Rev. Lett.* **111**, 070402 (2013).
 - [3] P. Nozières, *EPL* **103**, 57008 (2013).
 - [4] H. Watanabe and M. Oshikawa, *Phys. Rev. Lett.* **114**, 251603 (2015).
 - [5] G. Floquet, *Ann. Sci. École Norm. Sup.* **12**, 47 (1883).
 - [6] J. H. Shirley, *Phys. Rev.* **138**, B979 (1965).
 - [7] R. Moessner and S. L. Sondhi, *Nat. Phys.* **13**, 424 (2017).
 - [8] D. V. Else, C. Monroe, C. Nayak, and N. Y. Yao, *Annu. Rev. Condens. Matter Phys.* **11**, 467 (2020).
 - [9] M. P. Zaletel, M. Lukin, C. Monroe, C. Nayak, F. Wilczek, and N. Y. Yao, *Rev. Mod. Phys.* **95**, 031001 (2023).
 - [10] R. Nandkishore and D. A. Huse, *Annu. Rev. Condens. Matter Phys.* **6**, 15 (2015).
 - [11] D. A. Abanin, E. Altman, I. Bloch, and M. Serbyn, *Rev. Mod. Phys.* **91**, 021001 (2019).
 - [12] D. V. Else, B. Bauer, and C. Nayak, *Phys. Rev. Lett.* **117**, 090402 (2016).
 - [13] V. Khemani, A. Lazarides, R. Moessner, and S. L. Sondhi, *Phys. Rev. Lett.* **116**, 250401 (2016).
 - [14] N. Y. Yao, A. C. Potter, I.-D. Potirniche, and A. Vishwanath, *Phys. Rev. Lett.* **118**, 030401 (2017).
 - [15] J. Zhang *et al.*, *Nature* **543**, 217 (2017).
 - [16] P. Frey and S. Rachel, *Sci. Adv.* **8**, eabm7652 (2022).
 - [17] C. J. Turner, A. A. Michailidis, D. A. Abanin, M. Serbyn, and Z. Papić, *Nat. Phys.* **14**, 745 (2018).
 - [18] D. Bluvstein *et al.*, *Science* **371**, 1355 (2021).
 - [19] N. Maskara, A. A. Michailidis, W. W. Ho, D. Bluvstein, S. Choi, M. D. Lukin, and M. Serbyn, *Phys. Rev. Lett.* **127**, 090602 (2021).
 - [20] B. Huang, T.-H. Leung, D. M. Stamper-Kurn, and W. V. Liu, *Phys. Rev. Lett.* **129**, 133001 (2022).
 - [21] D. A. Abanin, W. De Roeck, and F. Huvneers, *Phys. Rev. Lett.* **115**, 256803 (2015).
 - [22] T. Mori, T. Kuwahara, and K. Saito, *Phys. Rev. Lett.* **116**, 120401 (2016).
 - [23] D. A. Abanin, W. De Roeck, W. W. Ho, and F. Huvneers, *Phys. Rev. B* **95**, 014112 (2017).
 - [24] D. V. Else, B. Bauer, and C. Nayak, *Phys. Rev. X* **7**, 011026 (2017).
 - [25] T. N. Ikeda, S. Sugiura, and A. Polkovnikov, *Phys. Rev. Lett.* **133**, 030401 (2024).
 - [26] K. G. Wilson, *Phys. Rev. D* **10**, 2445 (1974).
 - [27] T. Sulejmanpasic, H. Shao, A. W. Sandvik, and M. Ünsal, *Phys. Rev. Lett.* **119**, 091601 (2017).
 - [28] B. Lake, A. M. Tsvelik, S. Notbohm, D. Alan Tennant, T. G. Perring, M. Reehuis, C. Sekar, G. Krabbes, and B. Büchner, *Nat. Phys.* **6**, 50 (2010).
 - [29] A. J. A. James, R. M. Konik, and N. J. Robinson, *Phys. Rev. Lett.* **122**, 130603 (2019).
 - [30] F. B. Ramos, M. Lencsés, J. C. Xavier, and R. G. Pereira, *Phys. Rev. B* **102**, 014426 (2020).
 - [31] M. Kormos, M. Collura, G. Takács, and P. Calabrese, *Nat. Phys.* **13**, 246 (2017).
 - [32] S. Birnkammer, A. Bastianello, and M. Knap, *Nat. Commun.* **13**, 7663 (2022).
 - [33] J. Tindall and D. Sels, *Phys. Rev. Lett.* **133**, 180402 (2024).
 - [34] M. Collura, A. De Luca, D. Rossini, and A. Lerose, *Phys. Rev. X* **12**, 031037 (2022).

- [35] L. Pavešić, D. Jaschke, and S. Montangero, Constrained dynamics and confinement in the two-dimensional quantum Ising model (2024), [arXiv:2406.11979](https://arxiv.org/abs/2406.11979).
- [36] A. Santini, G. E. Santoro, and M. Collura, *Phys. Rev. B* **106**, 134301 (2022).
- [37] K. Shinjo, K. Seki, T. Shirakawa, R.-Y. Sun, and S. Yunoki, Unveiling clean two-dimensional discrete time quasicrystals on a digital quantum computer (2024), [arXiv:2403.16718](https://arxiv.org/abs/2403.16718).
- [38] J. Tindall, M. Fishman, E. M. Stoudenmire, and D. Sels, *PRX Quantum* **5**, 010308 (2024).
- [39] B. Bollobás, *Modern Graph Theory*, Graduate Texts in Mathematics No. 184 (Springer, New York, 1998).
- [40] M. Leifer and D. Poulin, *Ann. Phys.* **323**, 1899 (2008).
- [41] R. Alkabetz and I. Arad, *Phys. Rev. Res.* **3**, 023073 (2021).
- [42] S. Sahu and B. Swingle, Efficient tensor network simulation of quantum many-body physics on sparse graphs (2022), [arXiv:2206.04701](https://arxiv.org/abs/2206.04701).
- [43] C. Guo, D. Poletti, and I. Arad, *Phys. Rev. B* **108**, 125111 (2023).
- [44] J. Tindall and M. Fishman, *SciPost Phys.* **15**, 222 (2023).
- [45] D. V. Else, W. W. Ho, and P. T. Dumitrescu, *Phys. Rev. X* **10**, 021032 (2020).
- [46] S. Autti, V. Eltsov, and G. Volovik, *Phys. Rev. Lett.* **120**, 215301 (2018).
- [47] G. He, B. Ye, R. Gong, C. Yao, Z. Liu, K. W. Murch, N. Y. Yao, and C. Zu, Experimental Realization of Discrete Time Quasi-Crystals (2024), [arXiv:2403.17842](https://arxiv.org/abs/2403.17842).
- [48] F. Jemini, A. Russomanno, J. Keeling, M. Schirò, M. Dalmonte, and R. Fazio, *Phys. Rev. Lett.* **121**, 035301 (2018).
- [49] G. Piccitto, M. Wauters, F. Nori, and N. Shammah, *Phys. Rev. B* **104**, 014307 (2021).
- [50] F. Carollo and I. Lesanovsky, *Phys. Rev. A* **105**, L040202 (2022).
- [51] X. Zhang *et al.*, *Nature* **607**, 468 (2022).
- [52] Y. Kim *et al.*, *Nature* **618**, 500 (2023).
- [53] F. Arute *et al.*, *Nature* **574**, 505 (2019).
- [54] X. Mi *et al.*, *Nature* **601**, 531 (2022).
- [55] A. D. King *et al.*, Computational supremacy in quantum simulation (2024), [arXiv:2403.00910](https://arxiv.org/abs/2403.00910).
- [56] L. Xiang *et al.*, *Nat. Commun.* **15**, 8963 (2024).
- [57] S. Taie, H. Ozawa, T. Ichinose, T. Nishio, S. Nakajima, and Y. Takahashi, *Sci. Adv.* **1**, e1500854 (2015).
- [58] A. Periwal, E. S. Cooper, P. Kunkel, J. F. Wienand, E. J. Davis, and M. Schleier-Smith, *Nature* **600**, 630 (2021).
- [59] M. Lebrat, A. Kale, L. H. Kendrick, M. Xu, Y. Gang, A. Nikolaenko, S. Sachdev, and M. Greiner, Ferrimagnetism of ultracold fermions in a multi-band Hubbard system (2024), [arXiv:2404.17555](https://arxiv.org/abs/2404.17555).
- [60] S. Choi *et al.*, *Nature* **543**, 221 (2017).
- [61] B. Buča, J. Tindall, and D. Jaksch, *Nat. Commun.* **10**, 1730 (2019).
- [62] P. Kongkhambut, J. Skulte, L. Mathey, J. G. Cosme, A. Hemmerich, and H. Keßler, *Science* **377**, 670 (2022).
- [63] I. Carraro-Haddad, D. L. Chafatinos, A. S. Kuznetsov, I. A. Papuccio-Fernández, A. A. Reynoso, A. Bruchhausen, K. Biermann, P. V. Santos, G. Usaj, and A. Fainstein, *Science* **384**, 995 (2024).
- [64] K. Seibold, R. Rota, and V. Savona, *Phys. Rev. A* **101**, 033839 (2020).
- [65] iTensorNetworks.jl, <https://github.com/mtfishman/ITensorNetworks.jl> (2024).
- [66] J. Bezanson, A. Edelman, S. Karpinski, and V. B. Shah, *SIAM Rev.* **59**, 65 (2017).
- [67] M. Fishman, S. White, and E. Stoudenmire, *SciPost Phys. Codebases*, 4 (2022).

End Matter

Appendix A: Convergence of BP-iTNS results

To validate our BP-iTNS results obtained for the unit cell of an infinite lattice, we provide in Figure 5(a) a scaling analysis of the result of Fig. 2 for finite systems composed of $L \times L$ decorated hexagons for $L = \{1, 2, 3, 4\}$, corresponding to $N = \{12, 35, 68, 111\}$ qubits. As proven in more detail in Ref. [33], this illustrates that the BP approximation converges rapidly with system size in both the time-crystalline and thermalizing regimes. The inset shows a repetition of Fig. 3(c) but measured in the bulk of a 111-site system composed of 4×4 decorated hexagons, illustrating the survival of bipartite DTC order in finite systems. In infinite lattices represented by the $K_{2,z}$ unit cell, we have confirmed that bipartite DTC order is robust w.r.t. symmetry-broken initial states of the form $\bigotimes_i^{z+2} |\sigma_i\rangle$, with $\sigma_i = \uparrow\downarrow$ the Z -polarized state of a qubit in the unit cell.

As discussed in the main text and shown in Fig. 2(e), the lifetime of the prethermal DTC scales exponentially with $1/|\theta_x - \pi|$. To further illustrate the convergence of our results during the prethermal stage, we show in Fig. 5(b) the mean magnetization in the N -qubit system averaged over several numbers t/τ of Floquet cycles,

$$\bar{Z} = \frac{1}{n_\tau N} \sum_{n=1}^{t/\tau} \sum_{j=1}^N \langle \psi(n\tau) | (-1)^n Z_j | \psi(n\tau) \rangle. \quad (\text{A1})$$

While the magnetization converges rapidly in the DTC regime $\theta_x \rightarrow \pi$, the thermalizing regime is characterized by a slow decay, consistent with the eventual disappearance of DTC order at long times. The field strength θ_x^* of the crossover between these regimes, indicated in Fig. 2(d), is inferred from the convergence in time of the finite entanglement scaling. As shown in Fig. 5(c), the slope of the extrapolation reaches a maximum in the intermediary regime, which converges to $\theta_x^* \approx 0.73$ with

increasing number of Floquet cycles.

Appendix B: State vector simulation

For small systems, the dynamics generated by the Floquet unitary can be evaluated exactly by the direct application of one- and two-qubit gates on the state vector expressed in the computational basis of the 2^N -dimensional Hilbert space. This allows us to verify our conclusions obtained in the BP-iTNS approach with small graphs exhibiting a similar topology. To validate the existence of bipartite DTCs, we simulate the Floquet dynamics considered in Fig. 3 of the main text on complete z -regular graphs of a minimal size for $z = \{3, 4, 5\}$, with decorated edges. Shown in the top row are the magnetization dynamics on any of the equivalent qubits in the undecorated graphs comprising only the red nodes. For Floquet parameters $(\theta_J, \theta_x, \theta_z) = (0.5\pi, 0.85\pi, 0.4\pi)$, the magnetization lacks robust subharmonic order for graphs of any degree, and instead experiences a beating due to the presence of both a transverse and longitudinal field. Decorating the edges with additional (orange) qubits gives rise to the bipartite graphs shown in the top row of Fig. 6. For $z = 3$ (a) and $z = 4$ (b), these graphs have the same degrees of connectivity as the iTNS unit cells shown in Fig. 1. As in the main text, the resulting A - and B -sublattices now exhibit qualitatively different dynamics. Whereas the dynamics of the magnetization on the decorated qubits is unstable to any longitudinal field perturbation, the subharmonic response on z -connected qubits is stabilized for $z = 3$ [Fig. 6(a)] and $z = 5$ [Fig. 6(c)]. By contrast, time-crystalline order in the magnetization of a $z = 4$ bipartite graph [Fig. 6(b)] appears uniformly across both sublattices, as it does in the BP-iTNS approximation of an infinite Lieb lattice.

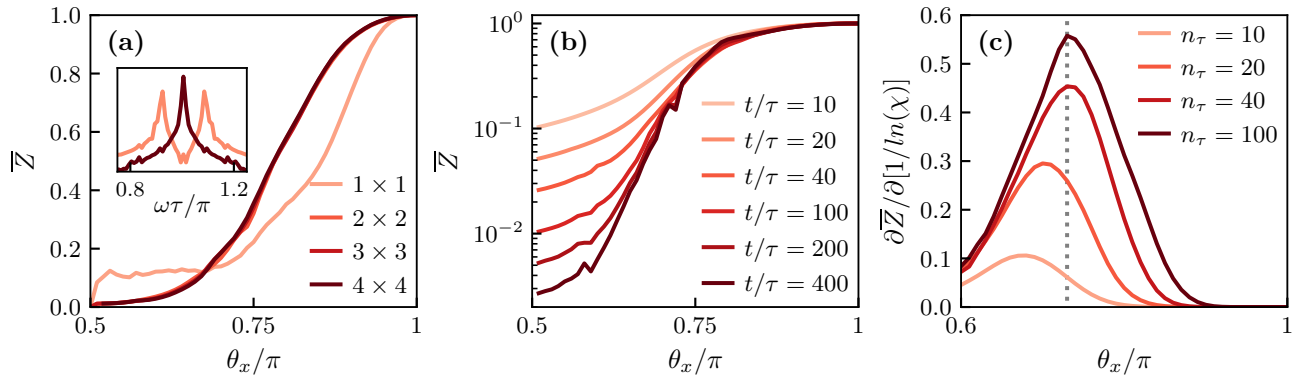


FIG. 5. **Scaling analysis of BP-iTNS results.** (a) Scaling of the time-averaged magnetization over 100 Floquet cycles with the number of unit cells in a finite decorated hexagonal lattice evaluated at $\chi = 80$. The inset shows the same result as Fig. 3(c) evaluated in the bulk of a 111-site system composed of 4×4 decorated hexagons. (b) Convergence of the magnetization in the BP-iTNS with the number of cycles at $\chi = 160$. (d) Evolution of the slope in the $\chi \rightarrow \infty$ extrapolation shown in Fig. 2.

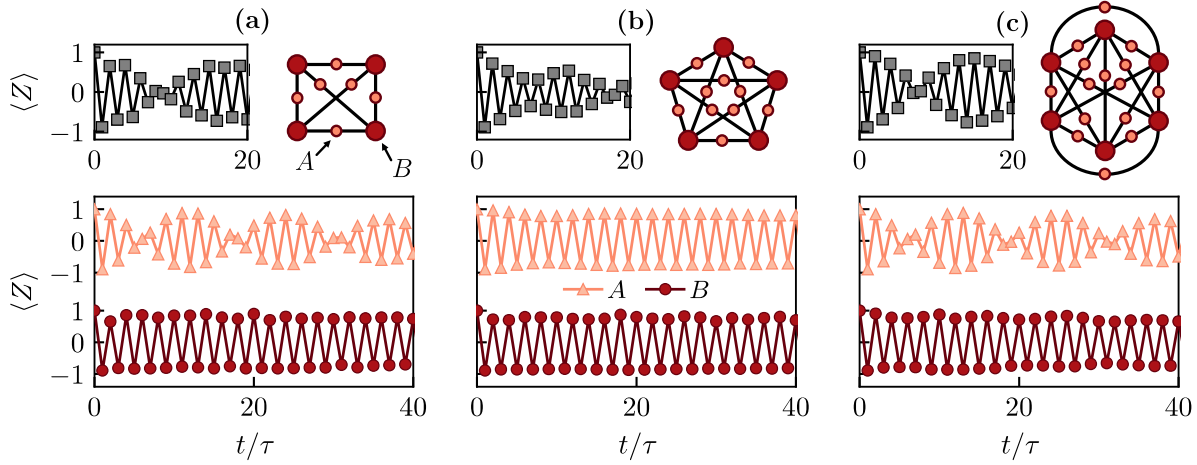


FIG. 6. **Bipartite rigidity in decorated regular graphs.** Exact dynamics of the magnetization $\langle Z \rangle$ generated by the Floquet unitary (3) with rotation angles $(\theta_x, \theta_z) = (0.85\pi, 0.4\pi)$ as in Fig. 3(c), on a 3-regular (a), 4-regular (b) and 5-regular graph. The top row shows the dynamics for the undecorated graphs (i.e., in absence of the orange nodes); the bottom row shows the dynamics on the A and B -qubits of the bipartite decorated graphs. The interaction strength θ_J was taken to be $\pi/2$ (a,c) and $\pi/3$ (b), within the DTC regime of the respective decorated graphs.